ELSEVIER

Dynamics of Atmospheres and Oceans 27 (1997) 301–332

dynamics of atmospheres and oceans

Extended Kalman filtering for vortex systems. Part I: Methodology and point vortices

Kayo Ide *, Michael Ghil

Department of Atmospheric Sciences and Institute of Geophysics and Planetary Physics, University of California, Los Angeles, CA 90095-1565, USA

Received 13 February 1996; revised 18 July 1996; accepted 18 July 1996

Abstract

Planetary flows—atmospheric and oceanic—are approximately two-dimensional and dominated by coherent concentrations of vorticity. Data assimilation attempts to determine optimally the current state of a fluid system from a limited number of current and past observations. In this two-part paper, an advanced method of data assimilation, the extended Kalman filter, is applied to the Lagrangian representation of a two-dimensional flow in terms of vortex systems. Smaller scales of motion are approximated here by stochastic forcing of the vortices.

In Part I, the systems studied have either two point vortices, leading to regular motion or four point vortices and chaotic motion, in the absence of stochastic forcing. Numerical experiments are performed in the presence or absence of stochastic forcing. Point-vortex systems with both regular and chaotic motion can be tracked by a combination of Lagrangian observations of vortex positions and of Eulerian observations of fluid velocity at a few fixed points. Dynamically, the usual extended Kalman filter tends to yield insufficient gain if stochastic forcing is absent, whether the underlying system is regular or chaotic. Statistically, the type and accuracy of observations are the key factors in achieving a sufficiently accurate flow description. A simple analysis of the update mechanism supports the numerical results and also provides geometrical insight into them. In Part II, tracking of Rankine vortices with a finite core area is investigated and the results are used for observing-system design. © 1997 Elsevier Science B.V.

1. Introduction

Data assimilation is a technique that describes the state of a dynamical system, subject to possible stochastic forcing, using limited knowledge about the system—such

* Corresponding author.

PII S0377-0265(97)00016-X

as its underlying deterministic dynamics and partial observations subject to measurement error. Using a suitable numerical scheme, the complete state of the system can be 'forecast' according to its underlying deterministic equations, from a given initial state. On the other hand, observations, which represent the true system perturbed by possible noise, may be available occasionally as a function of a small subset of the system variables. Merging a forecast from an earlier, imperfectly known initial state and current observations, data assimilation updates the system with the available observations to provide an 'analyzed' state by optimizing the expected difference between the 'analyzed' and 'true' state of the system (Bengtsson et al., 1981; Daley, 1991). Successful data assimilation depends on a good balance between the accuracy of its dynamical (forecast) and statistical (optimization) aspects. If the underlying dynamics of a system is not fully known, then data assimilation may help develop a model of the system via parameter identification (Smedstad and O'Brien, 1991; Hao and Ghil, 1995).

There are many fields in science and technology which heavily involve data assimilation (Panel on Model-Assimilated Data Sets for Atmospheric and Oceanic Research, 1991). In the fluid dynamics community for example, meteorologists have been using several data assimilation techniques for operational numerical weather prediction (NWP) and studies of atmospheric dynamics (Daley, 1991). Atmospheric models are often described as infinite-dimensional, continuum systems governed by partial differential equations (PDEs), such as the so-called primitive equations or the quasi-geostrophic equations. Numerical schemes for these models are often given in terms of finite-dimensional systems of ordinary differential equations (ODEs) in an Eulerian frame by discretizing the PDEs with respect to space. By integrating these finite-dimensional systems of ODEs, the atmospheric state is forecast in time. At the same time, abundant data regarding the actual atmospheric state such as temperature and velocity measurements from ground-based, airborne or satellite-borne instruments have become available. Techniques commonly used in meteorological data assimilation include so-called optimal interpolation (Gandin, 1965; Lorenc, 1981), variational methods (Sasaki, 1970; Provost and Salmon, 1986; Talagrand and Courtier, 1987), and Kalman filtering (Ghil et al., 1981).

The main goals of oceanographic data assimilation are different from meteorological data assimilation, emphasizing the investigation of fundamental ocean dynamics rather than prediction (Ghil and Malanotte-Rizzoli, 1991). Unlike atmospheric dynamics, for which models are well adapted to arbitrary regions of the earth, study of basic ocean dynamics is still actively in progress. Moreover, oceanographic data are often not given directly in terms of the model variables and are observed much less frequently and nonuniformly over the ocean as compared with the atmospheric data. Hence the challenge of oceanographic data assimilation is to help build suitable models which fit oceanographic data reasonably well.

Most data assimilation studies in meteorology and oceanography so far have been performed in an Eulerian frame in the sense that state variables are computed on fixed grids in space. When the flow can be represented by a few isolated vortices, however, assimilating the state of the fluid in an Eulerian frame may be computationally more expensive as well as less accurate. Localized coherent vortices are common phenomena in both meteorology and oceanography (McWilliams, 1991). For example, atmospheric

blocking in the mid-latitude troposphere can be represented by a persistent dipole vortex structure (McWilliams, 1980), and Gulf Stream rings are nearly axisymmetric vortices generated by the breaking of a meander from the Gulf Stream (Robinson, 1983). For such flows, tracking vortices is far more efficient and accurate in describing the 'macroscopic aspects' of flow dynamics. To analyze flows with coherent structures, Mariano (1990) suggested a technique to estimate consistently the isopleths, or contours, of a given flow from two or more independent information sources, whether they be observations or numerical forecasts.

In this study, we investigate the performance of data assimilation for simple vortex systems in a barotropic flow where the flow dynamics is described in a Lagrangian frame. The description is in terms of point vortices in Part I of the study and in terms of Rankine vortices in Part II. Although point-vortex and Rankine-vortex systems have much fewer degree of freedoms than an Eulerian description of the same flow fields, their dynamics is nonlinear and exhibits various types of motion, regular or chaotic. To deal with nonlinearity in these vortex systems, the extended Kalman filter (EKF) is chosen in the present study (Jazwinski, 1970; Ghil et al., 1981). The EKF is a nonlinear extension of the Kalman (1960) filter that had originally been developed for linear systems (Kalman and Bucy, 1961). Miller et al. (1994) investigated several data assimilation techniques for highly nonlinear systems, including a higher-moment EKF. Like all sequential data assimilation methods, the EKF has two ingredients: forecast and update. This two-part paper mainly focuses on the latter and addresses, in particular, observing-system design; issues concerning the former are discussed by Ide and Ghil (1997b).

The nature, distribution and accuracy of observations are important factors in the performance of data assimilation, as is the description of the system's dynamics. The observations may be linear or nonlinear, Eulerian or Lagrangian functions of the (discretized) field variables. In Part I of this study, we focus on general characteristics of vortex-system tracking using the EKF on point-vortex systems. We analytically demonstrate some basic update mechanisms in barotropic flow and point out certain potential problems in the light of the system's dynamics and observations. In Part II (Ide and Ghil, 1997a), we introduce a Rankine-vortex model for the flow dynamics to overcome some of these problems and propose criteria on the observations that, if met, will overcome the remaining problems encountered in Part I.

Part I of this paper is organized as follows. In Section 2 we give a quick review of the EKF, along with basic concepts of sequential estimation theory and its application to point-vortex systems. Two types of observations, Eulerian and Lagrangian, that we use are introduced. Numerical results of applying the EKF appear in Section 3. They include experiments using the EKF with both types of observations, on a two-point vortex system and a four-point vortex system, in the absence and presence of stochastic forcing. In Section 4 we explain analytically the update mechanisms acting when various types of observations are used, including some not illustrated by the numerical experiments in this paper. The analysis gives geometrical insight into the update mechanism, showing how vortex positions are affected by the observations. Brief concluding remarks are contained in Section 5. Two appendices give complete derivations of analytical results.

2. Formulation of the model and the method

2.1. Review of the extended Kalman filter (EKF)

In this section, we give a brief review of the EKF method in an N-dimensional vector space for continuous-time systems. This approach is more appropriate for the theoretical treatment of vortex systems than the discrete-time approach, since in many instances analytical, and hence sharper, results are possible. The EKF formulation for discrete-time fluid systems can be found by now in many places in the meteorological or oceanographic literature (e.g. Ghil et al., 1981, or Miller et al., 1994).

We first define a 'true' system and observations on it. The true system, including unresolved subgrid-scale processes, is denoted by superscript 't', and is assumed to be governed by a nonlinear stochastic differential equation,

$$d\mathbf{x}^t = \boldsymbol{f}(\mathbf{x}^t)dt + d\mathbf{q}^t, \tag{1a}$$

$$\mathbf{q}^t \sim \mathcal{N}(0_N, \mathbf{Q}^t), \tag{1b}$$

where $\mathbf{x}$ is an N-vector describing the state of the system, $\mathbf{f}$ is the N-vector of underlying deterministic transition functions, $\mathbf{q}$ is an N-dimensional Wiener process whose increments have mean zero and covariance matrix $\mathbf{Q} = E[\mathbf{q}\mathbf{q}^T]$, $E[\cdot]$ is an expectation operator, and $(\cdot)^T$ is the transpose of a (column) vector. Numerically, the evolution of the true state $\mathbf{x}^t$ is obtained by using a stochastic differential-equation integrator based on a generalization of Runge–Kutta methods (Greenside and Helfand, 1981); Miller et al. (1994) used a second-order two-step scheme based on a slightly different approach (see their Appendix A).

While the true state $\mathbf{x}^t$ evolves according to Eqs. (1a) and (1b), several observations regarding this system become available. At time t_j, an M_j-vector of observations $\mathbf{b}_j^o$ which contain white noise $\mathbf{w}_j$ is measured

$$\mathbf{b}_j^o = \mathbf{b}_j^t + \mathbf{w}_j^t, \tag{2a}$$

where

$$\mathbf{b}_j^t = \mathbf{h}_j\left(\mathbf{x}^t(t_j)\right), \tag{2b}$$

$$\mathbf{w}_j^t \sim \mathcal{N}\left(0_{M_j}, \mathbf{R}_j^t\right), \tag{2c}$$

$\mathbf{h}_j$ is an M_j-vector of observation functions that depend on the state variables $\mathbf{x}$ and may vary in number and nature at each update time, $\mathbf{R}_j = E[\mathbf{w}_j\mathbf{w}_j^T]$ is the $M_j \times M_j$ covariance matrix of the white-noise process $\boldsymbol{w}_j$ with mean zero, and subscript 'j' and superscript 'o' denote time t_j and 'observation', respectively. Observations $\{\mathbf{b}_j^o: j = 1, \ldots, L\}$ available L times during the evolution of $\mathbf{x}^t$, are the only data known to us regarding the true system. Note that $\mathbf{f}$ and $\mathbf{h}$ may be nonlinear functions of the state vector $\mathbf{x}$.

The goal of successful assimilation is to predict the state variables as accurately as possible by minimizing the expected error, given only limited knowledge regarding the true system. The EKF achieves this goal by combining dynamical and statistical aspects

of the system. It takes two successive steps, i.e. forecast and update. The EKF first forecasts the state vector $\mathbf{x}^{\mathrm{f}}$ according to the underlying deterministic equations, together with its error covariance matrix $\mathbf{P}^{\mathrm{f}}$, where superscript 'f' stands for 'forecast'. The forecast of the state itself is part of any prediction or simulation; the forecast of the 'error bars' of the state is useful in general but critical in data assimilation. When observations become available, the EKF updates the state variables to obtain optimized $\mathbf{x}^{\mathrm{a}}$ and $\mathbf{P}^{\mathrm{a}}$; the 'analyzed' $\mathbf{x}^{\mathrm{a}}$ and $\mathbf{P}^{\mathrm{a}}$ become the initial data for the next forecast. The repetition of these two steps in time gives its name to sequential estimation theory, of which the EKF is an important result.

We outline the statistical aspect of sequential estimation theory for a scalar variable x^{t} as a simple example. Suppose at $t = t_j$, we have two representations x_j^{f} and x_j^{o} of x_j^{t}, whose variances are Σ_j^{f} and Σ_j^{o}, respectively,

$$\left(\Sigma_j^{\mathrm{f,o}}\right)^2 = E\left[\left(x_j^{\mathrm{f,o}} - x_j^{\mathrm{t}}\right)\left(x_j^{\mathrm{f,o}} - x_j^{\mathrm{t}}\right)\right].$$

Assuming that the two representations are linear in x_j^{t}, unbiased and uncorrelated, the optimal estimate x_j^{a} of x_j^{t} is obtained by minimizing the mean-square error estimate J_j,

$$J_j \equiv E\left[\left(x_j^{\mathrm{a}} - x_j^{\mathrm{t}}\right)\left(x_j^{\mathrm{a}} - x_j^{\mathrm{t}}\right)\right].$$

The minimum $J_{j|\min}$

$$J_{j|\min} = \left[1 - \frac{\left(\Sigma_j^{\mathrm{f}}\right)^2}{\left(\Sigma_j^{\mathrm{o}}\right)^2 + \left(\Sigma_j^{\mathrm{f}}\right)^2}\right]\left(\Sigma_j^{\mathrm{f}}\right)^2$$

is achieved when

$$x_j^{\mathrm{a}} = x_j^{\mathrm{f}} + \frac{\left(\Sigma_j^{\mathrm{f}}\right)^2}{\left(\Sigma_j^{\mathrm{o}}\right)^2 + \left(\Sigma_j^{\mathrm{f}}\right)^2}\left(x_j^{\mathrm{o}} - x_j^{\mathrm{f}}\right).$$

The mathematical formulation of the EKF for a stochastic process given by Eqs. (1a) and (1b), together with observations given by Eqs. (2a), (2b) and (2c), is as follows (Gelb, 1974, Ghil, 1989). The EKF first forecasts the state vector $\mathbf{x}^{\mathrm{f}}$ and its error covariance matrix $\mathbf{P}^{\mathrm{f}}$,

$$\mathbf{P}^{\mathrm{f}} \equiv E\left[\left(\mathbf{x}^{\mathrm{f}} - \mathbf{x}^{\mathrm{t}}\right)\left(\mathbf{x}^{\mathrm{f}} - \mathbf{x}^{\mathrm{t}}\right)^T\right].$$

The forecast is obtained by solving the underlying deterministic equations numerically or analytically for a forecast interval, i.e. the time interval between two successive observations:

$$\frac{\mathrm{d}\mathbf{x}^{\mathrm{f}}}{\mathrm{d}t} = \mathbf{f}\left(\mathbf{x}^{\mathrm{f}}\right), \tag{3a}$$

$$\frac{\mathrm{d}\mathbf{P}^{\mathrm{f}}}{\mathrm{d}t} = \mathbf{F}^{\mathrm{f}}\mathbf{P}^{\mathrm{f}} + \left(\mathbf{P}^{\mathrm{f}}\right)^T\mathbf{F}^{\mathrm{f}} + \mathbf{Q}^{\mathrm{f}}, \tag{3b}$$

here

$$F^{\mathrm{f}}_{k,l} = \left.\frac{\partial f_k}{\partial x_l}\right|_{\mathbf{x}=\mathbf{x}^{\mathrm{f}}}, \tag{3c}$$

f_k and x_l are the kth and lth components of $\mathbf{f}$ and $\mathbf{x}$, respectively, $\mathbf{Q}^{\mathrm{f}}$ is the (given or estimated) noise covariance for the forecast and $\mathbf{F}$ is the linearized transition matrix with subscripts 'k' and 'l' representing row and column identities, respectively. At time t_j, the system is updated using $\mathbf{x}^{\mathrm{f}}(t_j)$ and $\mathbf{b}^{\mathrm{o}}_j$, together with their estimated error-covariance matrices $\mathbf{P}^{\mathrm{f}}(t_j)$ and $\mathbf{R}^{\mathrm{o}}_j$, where $\mathbf{R}^{\mathrm{o}}_j$ is assumed known, so as to minimize the mean-square error J_j defined by

$$J_j \equiv tr\mathbf{P}^{\mathrm{a}}(t_j) = E\left[\left(\mathbf{x}^{\mathrm{a}}(t_j) - \mathbf{x}^{t}(t_j)\right)\left(\mathbf{x}^{\mathrm{a}}(t_j) - \mathbf{x}^{t}(t_j)\right)^{T}\right]. \tag{4}$$

For fully nonlinear dynamics $\mathbf{f}$ and observations $\mathbf{h}$, no algorithm that minimizes Eq. (4) with any generality and executes in finite time is known. The EKF is characterized by solving for the full nonlinear state evolution, cf. Eq. (3a), and by using successive linearizations about the currently estimated state to advance the error–covariance matrix, cf. Eqs. (3b) and (3c). It thus provides a consistent first-order approximation to the optimal estimate of the state $\mathbf{x}^{\mathrm{a}}(t_j)$ at the observation time t_j,

$$\mathbf{x}^{\mathrm{a}}(t_j) = \mathbf{x}^{\mathrm{f}}(t_j) + \mathbf{K}_j\left\{\mathbf{b}^{\mathrm{o}}_j - \mathbf{h}_j\left[\mathbf{x}^{\mathrm{f}}(t_j)\right]\right\} \tag{5a}$$

and of its error $\mathbf{P}^{\mathrm{a}}(t_j)$,

$$\mathbf{P}^{\mathrm{a}}(t_j) = \left(\mathbf{I}_N - \mathbf{K}_j\mathbf{H}_j\right)\mathbf{P}^{\mathrm{f}}(t_j) \tag{5b}$$

where (Jazwinski, 1970, Ghil and Malanotte-Rizzoli, 1991)

$$\mathbf{K}_j = \mathbf{P}^{\mathrm{f}}(t_j)\mathbf{H}^{T}_j\left[\mathbf{H}_j\mathbf{P}^{\mathrm{f}}(t_j)\mathbf{H}^{T}_j + \mathbf{R}^{\mathrm{o}}_j\right]^{-1}, \tag{5c}$$

$$H_{k,l}|_j = \left.\frac{\partial h_k}{\partial x_l}\right|_{\mathbf{x}=\mathbf{x}^{\mathrm{f}}(t_j)}. \tag{5d}$$

Here $\mathbf{K}_j$ is the $N\times M_j$ gain matrix, $\mathbf{H}_j$ is the $M_j\times N$ linearized observation matrix, and $\mathbf{I}_N$ denotes the $N\times N$ identity matrix; $\mathbf{x}^{\mathrm{a}}$ and $\mathbf{P}^{\mathrm{a}}$ become the initial data for the next forecast of $\mathbf{x}^{\mathrm{f}}$ and $\mathbf{P}^{\mathrm{f}}$, respectively, while $\mathbf{x}^{\mathrm{a}}(t) = \mathbf{x}^{\mathrm{f}}(t)$ and $\mathbf{P}^{\mathrm{a}}(t) = \mathbf{P}^{\mathrm{f}}(t)$ between observations, $t_j < t \le t_{j+1}$.

In general, performance of the EKF can be measured by several informative quantities such as: (1) evolution of $tr\mathbf{P}^{\mathrm{f,a}}$ that indicates the estimated least-square error; (2) evolution of selected components of $\mathbf{P}^{\mathrm{f,a}}$ that indicate how well the corresponding state variables are estimated in the least-square sense; and (3) comparison among the evolution of the true observed and estimated state variables and the corresponding terms in $\mathbf{P}^{\mathrm{f,a}}$ and that helps evaluate the actual performance of the EKF and its credibility.

The dynamical aspect of the data assimilation process is the forecast and is given by Eqs. (3a), (3b) and (3c), while the statistical aspect is the update and is given by Eqs. (5a), (5b), (5c) and (5d). Together, they yield the EKF method for estimating the state of the true system governed by Eqs. (1a) and (1b) subject to observations defined by Eqs.

(2a), (2b) and (2c). The EKF is, in fact, merely a consistent first-order approximation of the ideal data assimilation scheme for nonlinear systems; no finite-time numerical implementation of a truly optimal sequential scheme for such systems. In the presence of both initial uncertainty and system noise, is conceivable at present.

As discussed by Cohn (1993) and Miller et al. (1994), both the best sequential scheme (given computational and other implementation constraints) and the stability of its error covariance matrix remain important research topics to be addressed in the future. Recent developments of the ensemble forecast method (Toth and Kalnay, 1993; Buizza et al., 1993) hold great promise for medium-range weather forecasts and stimulated a new look at classical predictability results (Anderson, 1995; Legras and Vautard, 1996). In the rest of this two-part paper, we mainly focus on the optimization of observing-system design and thus emphasize the update aspect of the EKF. Issues concerning the forecast component of sequential data assimilation, such as the short-, medium-, and long-term evolution of prediction errors and the influence of stochastic forcing on them are discussed by Ide and Ghil (1997b).

2.2. Application to point-vortex systems

We now apply the EKF to a system of N point vortices. Our goal is to predict vortex positions accurately and to minimize the expected error, by using known underlying vortex dynamics and available observations, while the vortices evolve due to nonlinear interactions and also possibly due to stochastic forcing. The system's state variables, i.e. the vortex positions, can be represented in several ways. In this study, we treat the N vortex positions as N complex state variables, i.e. $z_v = \{z_{v,1}, z_{v,2}, \ldots, z_{v,N}\}$ is a complex-valued N-vector, $z_{v,l} = x_{v,l} + iy_{v,l}$ being the complex coordinate of vortex l.

The underlying deterministic dynamics for N point vortices is given by

$$\frac{dz^*_{v,l}}{dt} = f_{v,l}(z_v) = \sum_{n=1,n\neq l}^{N} \frac{\Gamma_n}{i2\pi} \frac{1}{z_{v,l} - z_{v,n}}, \quad el = 1,\ldots,N \tag{6}$$

where $z^*_{v,l}$ denotes the complex conjugate of $z_{v,l}$, $f_{v,l}$ is the underlying deterministic velocity function for vortex l, and Γ_n is the circulation of vortex n. The induced velocity around a point vortex is singular at the vortex and decays like $1/el$, where el is the distance from the vortex. Each vortex is advected with the local fluid velocity, which is a superposition of velocities induced by the other $N-1$ vortices in the flow. The forecast of the vortex positions z^f_v and of the error–covariance matrix $\mathbf{P}^f$ are obtained by integrating the deterministic equations of motion using the second-order Rung and Kutta scheme. Since a complex state variable consists of two scalar state variables, $\mathbf{P}^f$ is naturally decomposed into N^2 2×2 block elements whose (k, l)th element $\mathbf{P}^f_{kl}$ is given by

$$\mathbf{P}^f_{kl} = E\left[\begin{pmatrix} \Delta x_{v,k}\Delta x_{v,l} & \Delta x_{v,k}\Delta y_{v,l} \\ \Delta y_{v,k}\Delta x_{v,l} & \Delta y_{v,k}\Delta y_{v,l} \end{pmatrix}\right],$$

here

$$(\Delta x_{v,l}, \Delta y_{v,l}) = (\mathscr{R}, \mathscr{I})\left(z^f_{v,l} - z^t_{v,l}\right),$$

with $\mathscr{R}$ and $\mathscr{I}$ the real and imaginary parts of a complex number.

Similarly, the linearized transition matrix $\mathbf{F}^{\mathrm{f}}$ and the covariance matrix $\mathbf{Q}^{\mathrm{f}}$ may be decomposed into N^2 2×2 blocks. Assuming that the stochastic forcing for the state variables is given by zero-mean white noise, uncorrelated from one vortex to the other, the estimated covariance of stochastic forcing is:

$$\mathbf{Q}^{\mathrm{f}}_{kl} = \delta_{kl} q^{\mathrm{f}}_k \mathbf{I}_2, \quad k,l = 1,\ldots,N, \tag{7}$$

where q^{f}_k is the magnitude of the variance for each vortex, and δ_{kl} the Kronecker delta. With $\mathbf{F}^{\mathrm{f}}$ and $\mathbf{Q}^{\mathrm{f}}$ defined as above, the forecast $\mathbf{P}^{\mathrm{f}}$ is computed according to Eqs. (3a), (3b) and (3c).

Two types of observations are used in this paper. The subscript corresponding to the observation time is dropped for convenience. Observations $\mathbf{c}^{\mathrm{o}}$ consist simply in (a subset of) vortex('-center') positions (cf. Part II) given by the M_{v}-vector

$$\mathbf{c}^{\mathrm{o}} = \left\{c^{\mathrm{o}}_1, c^{\mathrm{o}}_2, \ldots, c^{\mathrm{o}}_{M_{\mathrm{v}}}\right\}, \tag{8a}$$

where

$$c^{\mathrm{o}}_k = h_{\mathrm{v},k}\left(z^{\mathrm{t}}_{\mathrm{v}}\right) + w^{\mathrm{t}}_{\mathrm{v},k}, \tag{8b}$$

$$h_{\mathrm{v},k}(z_{\mathrm{v}}) = z_{\mathrm{v},m}, \quad k = 1,\ldots,M_{\mathrm{v}}, \tag{8c}$$

$h_{\mathrm{v},k}$ is the complex observation function with subscripts 'v' and 'k' denoting 'vortex' and the kth observation, respectively, M_{v} is the number of observations of this type and m is the vortex identity which corresponds to the kth observation, with $1 \le m \le N$. Such Lagrangian measurements could be made by drifting buoys trapped in the 'eye' of a persistent eddy or by interpretation of satellite infrared imagery.

The other type of observations consists of the conjugate of the complex flow velocity $\mathbf{u}^{\mathrm{o}}$, measured at some given points, i.e. stations z_{s}:

$$\mathbf{u}^{\mathrm{o}} = \left\{u^{\mathrm{o}}_1, u^{\mathrm{o}}_2, \ldots, u^{\mathrm{o}}_{M_{\mathrm{s}}}\right\}, \tag{9a}$$

where

$$u^{\mathrm{o}}_k = h_{\mathrm{s},k}\left(z^{\mathrm{t}}_{\mathrm{v}}, z_{\mathrm{s},m}\right) + w^{\mathrm{t}}_{\mathrm{s},k}, \tag{9b}$$

$$h_{\mathrm{s},k} = \sum_{n=1}^{N} \frac{\Gamma_n}{i2\pi} \frac{1}{z_{\mathrm{s},m} - z_{\mathrm{v},n}}, \quad k = 1,\ldots,M_{\mathrm{s}}. \tag{9c}$$

$z_{\mathrm{s},m}$ is the position of the mth station, M_{s} is the number of velocity observations, subscript 's' denotes 'station' and $m = m(k)$ is the station identity which corresponds to the kth observation of this type. Such Eulerian measurements could be implemented in oceanography by fixed current meters, ship stations or by the remote tracking of natural or artificial 'features' transiting a given location (such as the cloud-track winds obtained in the atmosphere from geostationary satellites).

There are a total of $M = M_{\mathrm{v}} + M_{\mathrm{s}}$ complex observations $\mathbf{b}^{\mathrm{o}} = \{\mathbf{c}^{\mathrm{o}}, \mathbf{u}^{\mathrm{o}}\}$ associated with M observation functions $\mathbf{h} = \{\mathbf{h}_{\mathrm{v}}, \mathbf{h}_{\mathrm{s}}\}$. The two types of observations have certain features in common, as well as major differences. The most useful common characteristic is that $\mathbf{h}_{\mathrm{v}}$ and $\mathbf{h}_{\mathrm{s}}$ can both be written as analytic functions of the state variables z_{v}. As discussed in greater detail in Section 4.1, such analytic observation functions are

common for point-vortex systems. This property becomes useful in understanding geometrically the update mechanisms for various types of observations.

There are three major differences between position and velocity observations. First, $\mathbf{h}_v$ is Lagrangian while $\mathbf{h}_s$ is Eulerian. Second, $\mathbf{h}_v$ is linear while $\mathbf{h}_s$ is nonlinear in z_v. Finally, $\mathbf{h}_v$ is a function of only one state variable (single-state-variable function), whereas $\mathbf{h}_s$ is a function of all the state variables (multi-state-variable function). As $\mathbf{P}^f$ and $\mathbf{F}^f$ may be decomposed into 2×2 matrices, the linearized observation matrix $\mathbf{H}$ may also be decomposed into MN 2×2 matrices. Throughout this study, the observation errors are assumed to be uncorrelated, i.e.

$$\mathbf{R}^{t,o}_{kl} = \delta_{kl} r^{t,o}_k \mathbf{I}_2, \quad k,l = 1,\ldots,M, \tag{10}$$

where $r^{t,o}_k$ may be chosen either as a given function of the magnitude of the observation or as given constants.

3. Numerical results

3.1. Two-point vortex system

A system of two point vortices, in the absence of stochastic forcing, has a Hamiltonian with one degree-of-freedom. Hence its motion is regular; more precisely, it is periodic unless the two circulations have the same amplitude but opposite sign, in which case the motion is linear, parallel translation. If the system is subject to stochastic forcing, then the dynamics of the two vortices is no longer deterministic and their exact trajectories are unpredictable. In this subsection, we examine the performance of the EKF on a system of two point vortices, both in the absence and presence of stochastic forcing.

Since the underlying deterministic system is governed by a Hamiltonian with one degree-of-freedom, the two vortices may be assumed, without loss of generality, to have the same sign and equal circulations. At $t = 0$, the pair of vortices $z_{v,1}$ and $z_{v,2}$, with circulation $\Gamma = 1$, are located at (1, 0) and (−1, 0) respectively. The system has a natural period of ~ 160 time units. In each run with stochastic forcing, $q^f = 0.01$ for each forcing term in Eq. (7). The initial condition of p^f is assumed to equal r^o, reflecting the fact that the errors in the initial vortex positions are comparable to the observational ones.

Each Lagrangian observation of vortex position $\mathbf{c}^o = \{c^o_1, c^o_2\}$ is assumed to contain uncorrelated white noise in the x- and y-components with corresponding variances $r^o = 0.04$ in Eq. (10). Eulerian velocity observations $\mathbf{u}^o$ are taken to depend nonlinearly on both vortex positions. In this study, we choose three stations $z_{s,1}$, $z_{s,2}$, and $z_{s,3}$ at (0, 0), (0.9, 0), and (2, 0), as shown in Fig. 1, at which complex conjugate velocities $\mathbf{u}^o = \{u^o_1, u^o_2, u^o_3\}$ are measured. In the absence of stochastic forcing, $z_{s,1}$ is at the stagnation point (i.e. the velocity there is zero) and lies inside of both vortex trajectories, $z_{s,2}$ lies inside but close to the vortex trajectories, and $z_{s,3}$ is located outside of the vortex trajectories. The effect of the stations' position is discussed briefly in Section 3.2 here and in greater detail in Part II, as part of the general problem of observing-system

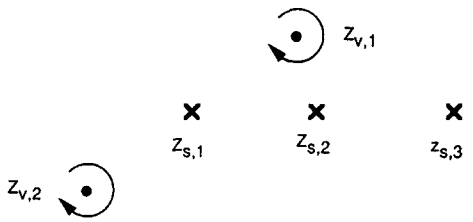

Fig. 1. Schematic diagram of two vortices (solid circles) and three stations (× signs).

design (Ghil and Ide, 1994). The velocity observations $\mathbf{u}^o$ are assumed to contain errors with a standard deviation of 20% of their true absolute values, i.e. $r_k^{i,o}$ in Eq. (10) are computed based on the magnitude of velocity observations.

This study is exploratory and does not claim to simulate in detail the behavior of known observing systems in meteorology or oceanography. As indicated at the end of Section 2.2 either Lagrangian or Eulerian observations could be implemented in a number of ways, each with its own error characteristics. The assumptions made about observing errors are thus taken rather arbitrarily, but on the difficult side of the range of possibilities.

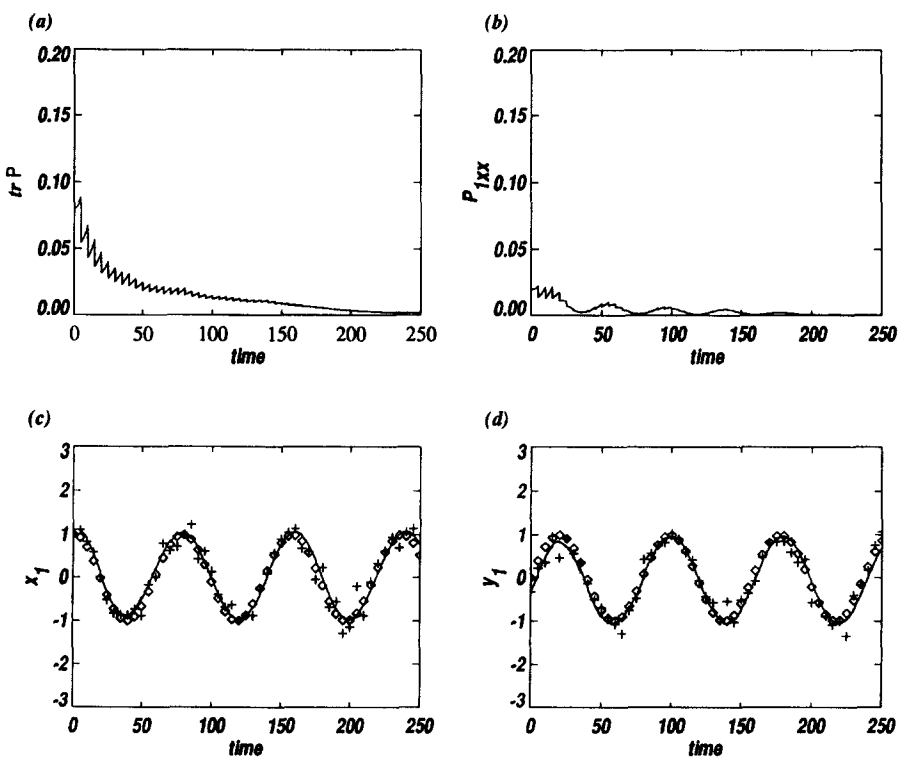

Fig. 2. The performance of the EKF for two point vortices without stochastic forcing, when observing their positions every 5 time units: (a) $tr\mathbf{P}$; (b) P_{1xx}; (c) x_1; (d) y_1.

There are thus a maximum of five available complex-valued observations and three possible combinations of observation types: $\mathbf{c}^o$ only, $\mathbf{c}^o$ as well as $\mathbf{u}^o$, and $\mathbf{u}^o$ only. In the following subsections, we examine the performance of the EKF using various types and combinations of observations, in the absence and presence of stochastic forcing. Results are shown in terms of $tr\mathbf{P}^{f,a}$ and some components of $\mathbf{P}^{f,a}$, as well as comparing the evolution of true, observed and estimated vortex positions.

3.1.1. No stochastic forcing

Figs. 2–5 show the typical performance of the EKF in the absence of stochastic forcing. The trace $\mathbf{P}^{f,a}$ of the error covariance matrix $\mathbf{P}^{f,a}$ represents the overall performance of the EKF, since the EKF is designed to minimize $tr\mathbf{P}^a$, cf. Eq. (4); P_{1xx} is the component of $\mathbf{P}$ giving the error covariance of the x-coordinate of vortex 1. Hereafter and in the figures we drop the superscripts 'f', 'a' and 'o' for convenience. The x- and y-coordinates of vortex 1 are plotted to show actual performance of the EKF. Solid curves correspond to the EKF estimation, open diamonds correspond to the true state of the system, and plus signs correspond to the (noisy) observations. The system is updated every 5 time units using the observations available for each run; in Fig. 3 the update is done only every 50 time units, i.e. about three times per rotation of the vortices around the stagnation point. In Figs. 2 and 3 both vortex positions are used,

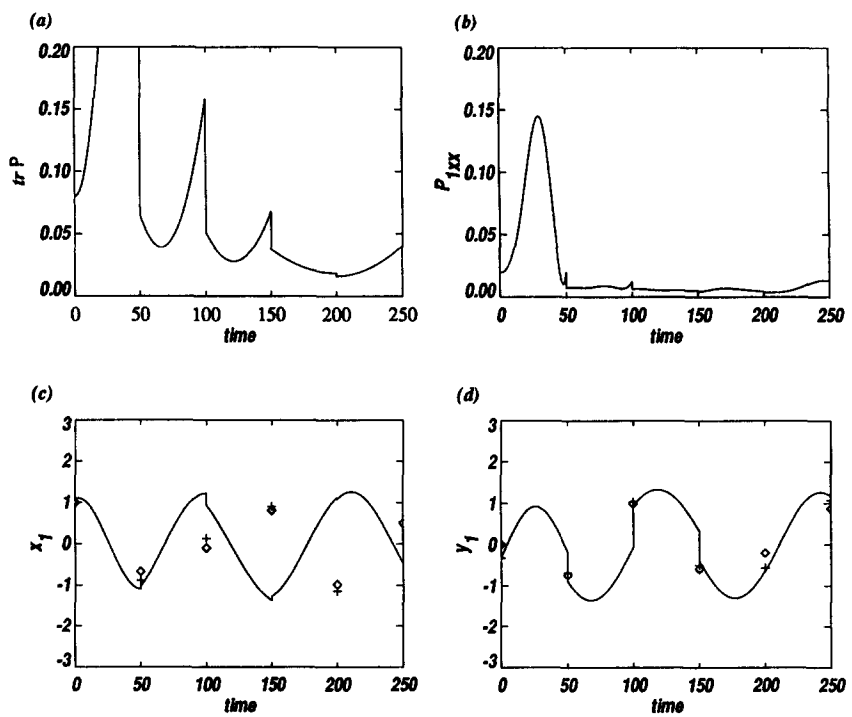

Fig. 3. The performance of the EKF for two point vortices without stochastic forcing, when observing their positions every 50 time units: (a) $tr\mathbf{P}$; (b) P_{1xx}; (c) x_1; (d) y_1.

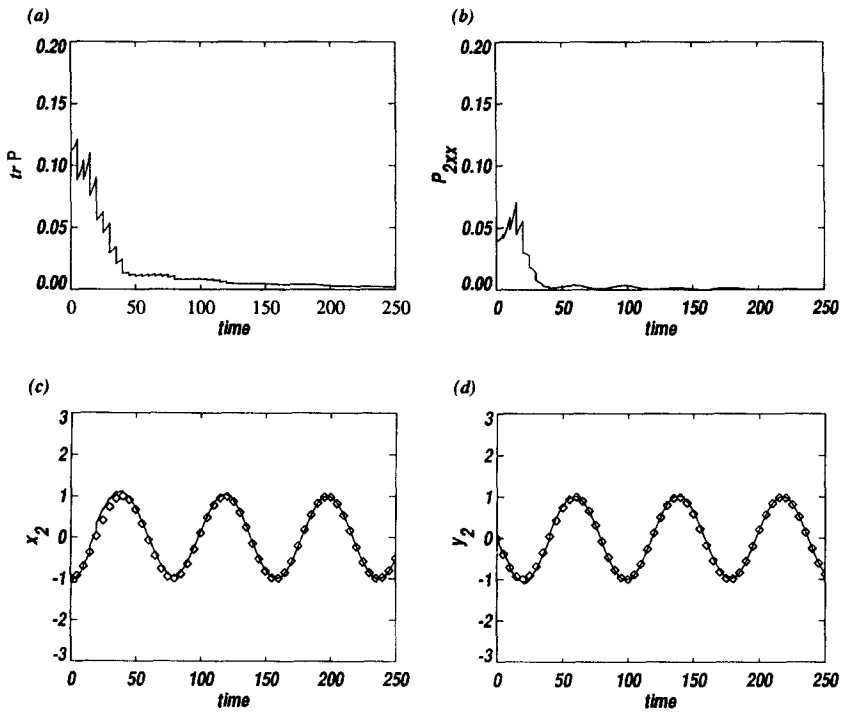

Fig. 4. The performance of the EKF for two point vortices without stochastic forcing, when observing vortex position c_1 and station velocity u_2 every 5 time units: (a) $tr\mathbf{P}$; (b) P_{2xx}; (c) x_2; (d) y_2.

i.e. $\mathbf{b} = \{c_1, c_2\}$, for each update, while Figs. 4 and 5 show updates using one vortex position and one velocity observation at $z_{s,1}$, i.e. $\mathbf{b} = \{c_1, u_2\}$ and $\mathbf{b} = \{c_1, u_1\}$, respectively.

Recall that the EKF estimates the system from one observation time to the next in two successive steps, i.e. forecast and update. EKF performance depends on consistency between the two steps. The main characteristic of the forecast process in the absence of stochastic forcing is the slow, periodically modulated growth of the components of $\mathbf{P}$. This is due to the regular motion of the vortices, since the growth rate is related to the eigenvalues of the system along a trajectory (Miller et al., 1994).

The efficiency of the update relies on how well $\mathbf{P}$ and $\mathbf{R}$ represent the forecast and observation errors, as well as on the number, type and accuracy of observations. Let us consider the update using $\mathbf{c}^o$ only. Fig. 2 shows an example of excellent tracking. Notice that, in the absence of stochastic forcing, $tr\mathbf{P}$ decays roughly like $1/t$ (compare Fig. 2 of Ghil et al., 1981), i.e. like the estimation variance of a scalar subject to n repeated uncorrelated observations having equal variance, with $n = t$. Thus knowledge of the Lagrangian flow dynamics and use of the EKF reduce the problem of flow-field estimation to that of scalar estimation, given a very small number of observations.

If, on the other hand, the growth of the components of $\mathbf{P}$ between observations is not large enough, frequent updates tend to make these components decay rapidly and hence

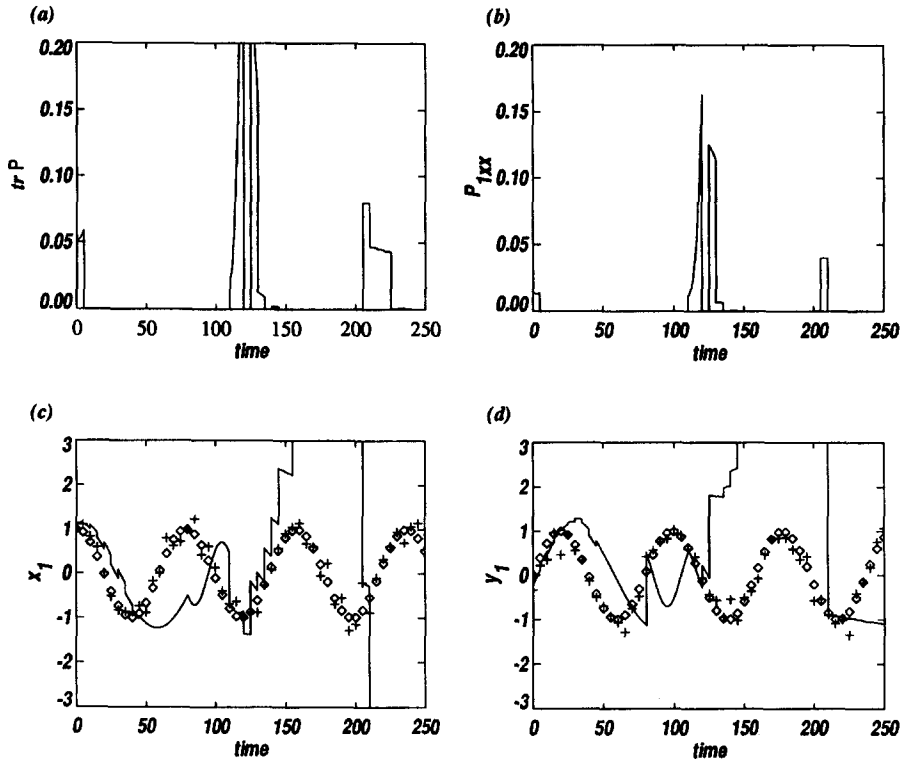

Fig. 5. Same as Fig. 4, but with velocity observation u_1: (a) $tr\mathbf{P}$; (b) P_{1xx}; (c) x_1; (d) y_1.

become quite small. Once the components of **P** become small as compared with the components of **R**, the gain **K** in Eqs. (5a), (5b), (5c) and (5d) at update time is insufficient and hence observations do not play a significant role in estimating the vortex positions (not shown, but see Fig. 3(a) of Miller et al., 1994). Hence, in the absence of stochastic forcing, when the vortex-position observations are frequent, the performance of the EKF depends on the accuracy of the last update before the components of **P** become too small compared with those of **R**. If the 'last significant' update at the end of the initial adjustment period fails to accurately estimate the vortex position, the estimated positions slowly but steadily drift away from the true ones due to nonlinear vortex interaction.

When the updates are much less frequent, the performance of the EKF depends on how well **P** and **R** represent the evolution of the system, as shown in Fig. 3. The components of **P** related to the y-coordinate of vortex 1 (not shown) are well represented and hence the estimated coordinate follows the true one faithfully; however, the component of **P** for the x-coordinate of the same vortex does not grow enough to affect the updating (Fig. 3(b)). The behavior of each component of **P** depends on the initial data as well as on the underlying nonlinear dynamics of the point-vortex system.

When only one of the two vortex positions is observed, the unobserved vortex

receives much smaller corrections at update time. A station-velocity observation can compensate for this, provided the initial guess for the vortex positions is good enough (see Fig. 4). Inaccurate initial data for the unobserved vortex result, however, not only in false estimation of its position but may also contaminate the estimation of the vortex position that is observed, through the interaction of the two. Again, gentle growth of **P** according to deterministic dynamics results in insufficient gain for the update. Once **P** becomes small with respect to **R**, new observations have almost no impact on the estimation. Hence accurate initial data for the vortex positions become an important factor for EKF performance.

As shown analytically in the next section and in Appendix A, Eulerian station velocity observations have advantages and disadvantages compared with Lagrangian vortex-position observations. An advantage is that, since velocity at an arbitrary fixed point depends on all the vortices, all vortices are updated by a single-station velocity observation. An important disadvantage is that the observation function $\mathbf{h}_s$ depends nonlinearly on the vortex position z_v and the influence of a velocity observation behaves like l^{-4}, where l is the distance between the station and a given vortex; hence the effect of such an observation has a strong singularity for small l and becomes very weak for large l. For Lagrangian vortex-position observation, if **P** is not a diagonal matrix, then the update using one vortex position will indeed change the positions of other vortices, though the effect may not be as significant as the one observed here. We are merely talking, however, about the simple analysis using the diagonal **P**, to explain the underlying update mechanism.

When station-velocity observations are added to observations of both vortex positions, the performance of the EKF does not change significantly, as long as the station is not located near a stagnation point of the field. Smaller velocity observations tend to accelerate the quick decay of the (estimated) components of **P**, while overall filter performance does not actually improve, due to the l^{-4} factor (see Section 4; the term most affected by l is d_{kl}^2 in Eq. (18)). If the observations include only one of both vortex positions and some velocity observations (Fig. 4), the unobserved vortex (Fig. 4(d)) is more accurately up-dated than in the absence of velocity observations. When, in addition to having position observations, a velocity station is located near a stagnation point, the filter may fail badly in tracking the vortices (Fig. 5). The mechanism for this misbehavior as well as its remedy, will be discussed in Section 4 here and Section 4 of Part II, respectively. When the observational data include only station velocities (not shown), the components of **P** do not decay rapidly, and hence the updates have greater impact on the estimation. The EKF thus performs reasonably well as long as the initial data are sufficiently accurate.

3.1.2. With stochastic forcing

In more realistic situations, when the system is subject to stochastic forcing, true motion of the two vortices is no longer simple rotation. Since the vortex positions are still forecast according to the underlying deterministic dynamics, the true and forecast positions of the vortices may drift apart during one updating interval even if their initial data are identical. On the other hand, the components of **P** will grow faster, so that they will no longer be underestimated with respect to those of **R**. Hence the performance of

the EKF is likely to be improved, while still depending strongly on the type and number of the observations and on the accuracy of **R** and **P**.

Figs. 6–8 are the counterpart of Figs. 2, 3 and 5 in the presence of stochastic forcing. The true motion of the vortices in this case is computed by the appropriate stochastic generalization of the second-order Runge–Kutta method (Greenside and Helfand, 1981). Although the motion is much more complicated than in the purely deterministic case, the EKF performs in all three cases better in capturing the overall dynamics. This is true when both vortex positions are observed (Figs. 6 and 7), but even more strikingly so when only one vortex position and one station velocity are observed (Fig. 8).

For the time interval shown in Fig. 7, the stochastic forcing (although it has mean zero, cf. Eqs. (1a) and (1b)) happens to bring the two vortices closer to each other and thus increase systematically their velocity of rotation around the stagnation point. Hence the updates while separated by the same interval of 50 time units as in Fig. 3, are more infrequent compared with the average period of rotation than in the purely deterministic case. Still, the growth of the components of **P** is fast enough for the estimation to almost recover the true positions at every update. If some component of **P** is small at update time, then the corresponding state variable may not be influenced by it. In Fig. 7, the system recovers the x-coordinate of vortex 1 quite well while the y-coordinate (P_{1yy}, not shown) follows the observations less closely. Unlike the situation where stochastic

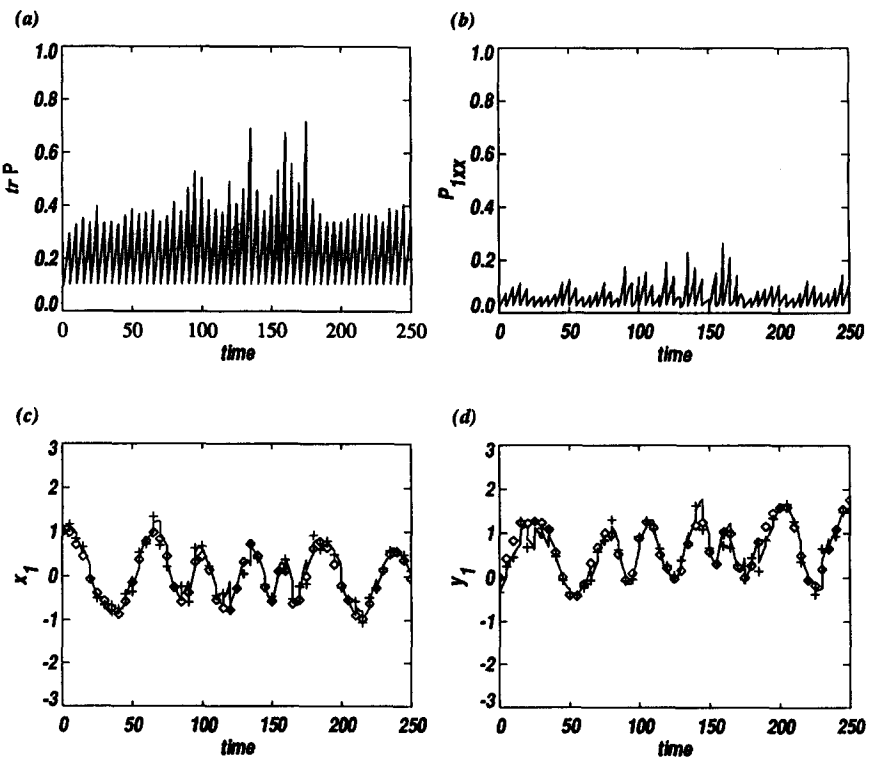

Fig. 6. Same as Fig. 2, but with stochastic forcing.

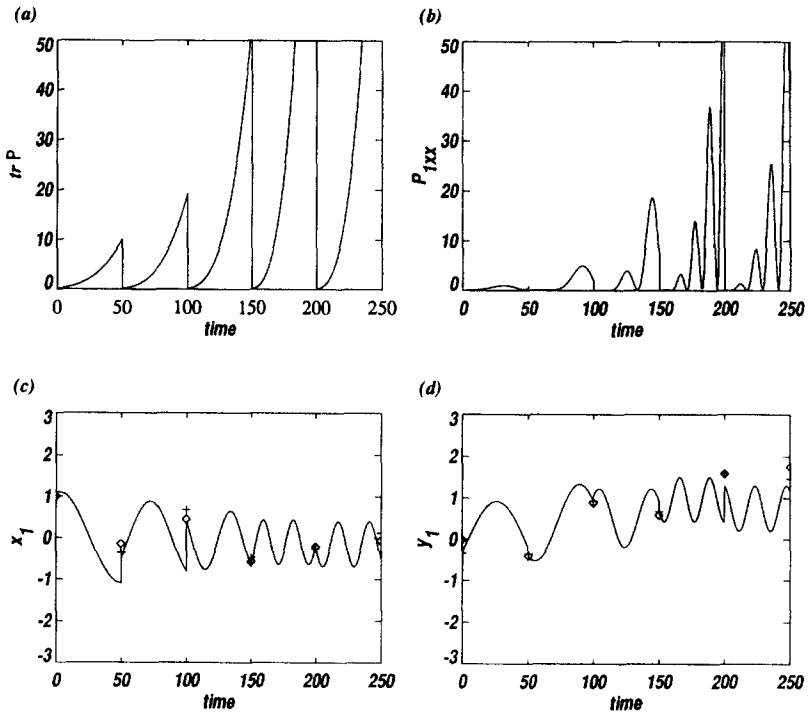

Fig. 7. Same as Fig. 3, but with stochastic forcing.

forcing is absent, the components of **P** can increase again and hence recover the observed value in the following updates (not shown).

Adding velocity observations to both vortex positions being observed does not change substantially the overall performance of the EKF (not shown). Due to stochastic forcing, $z_{s,1}$ is no longer a stagnation point and hence updates using u_1 do not fail dramatically (Fig. 8), as they did before (Fig. 5), given only one observation of vortex position.

3.2. Four-point vortex system

It is well known that a deterministic system of four or more point vortices in the plane may exhibit chaotic dynamics (Aref, 1984). In this subsection we examine the performance of the EKF when the deterministic system is chaotic. At $t = 0$, four vortices are located at positions that are slightly perturbed away from the corners of the 1.6×0.4 rectangle centered at the origin. Due to the perturbation from perfect symmetry in initial data, the vortices undergo deterministically chaotic motion. In each run in which stochastic forcing is present, q' in Eq. (7) is assumed to be 0.01 as before.

The observing patterns considered include Lagrangian measurement of the vortex positions and Eulerian velocity measurements at the same three stations as in the previous subsection. The relative positions of the stations with respect to the vortex

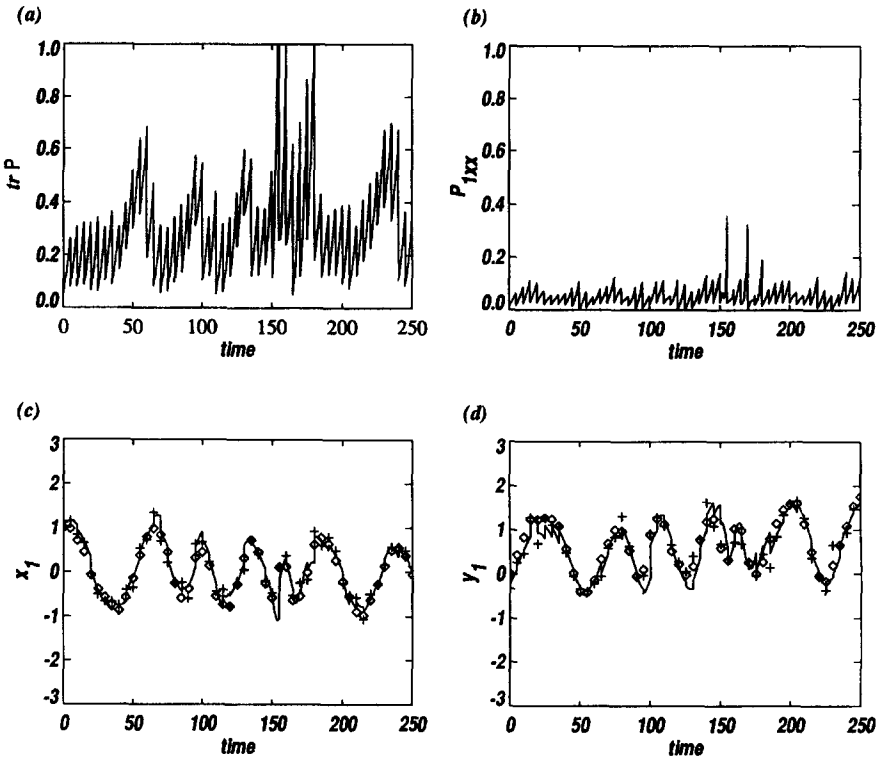

Fig. 8. Same as Fig. 5 but with stochastic forcing.

paths are also the same as before. The exact positioning of stations is less important in the physically more realistic, and hence important, case of four or more vortices. In this case, the nonlinear interaction of the vortices leads to their trajectories being irregular and covering an area of the plane more or less uniformly (see Fig. 4 in Part II). Hence, an equal number of stations in a different, but likewise fixed configuration will achieve comparable accuracy in tracking. The effect of optimal observing-system design on accuracy will be discussed in Part II.

Note that $z_{s,1}$ is no longer at the exact stagnation point, even in the purely deterministic case. There are now a total of at most seven available complex-valued observations of the two types. Both types of observations are assumed to contain white noise as in the previous subsection. Since the basic mechanism of update is similar to that for the two point-vortex system, the main difference in the EKF estimation process is due to the more complex underlying dynamics of the present system.

3.2.1. No stochastic forcing

Since the motion of the four point vortices exhibits deterministic chaos, the performance of the EKF in this case depends sensitively on how accurately z_v^a represents z_v^t at each update. Small differences between z_v^a and z_v^t may result in totally different trajectories even after a short time.

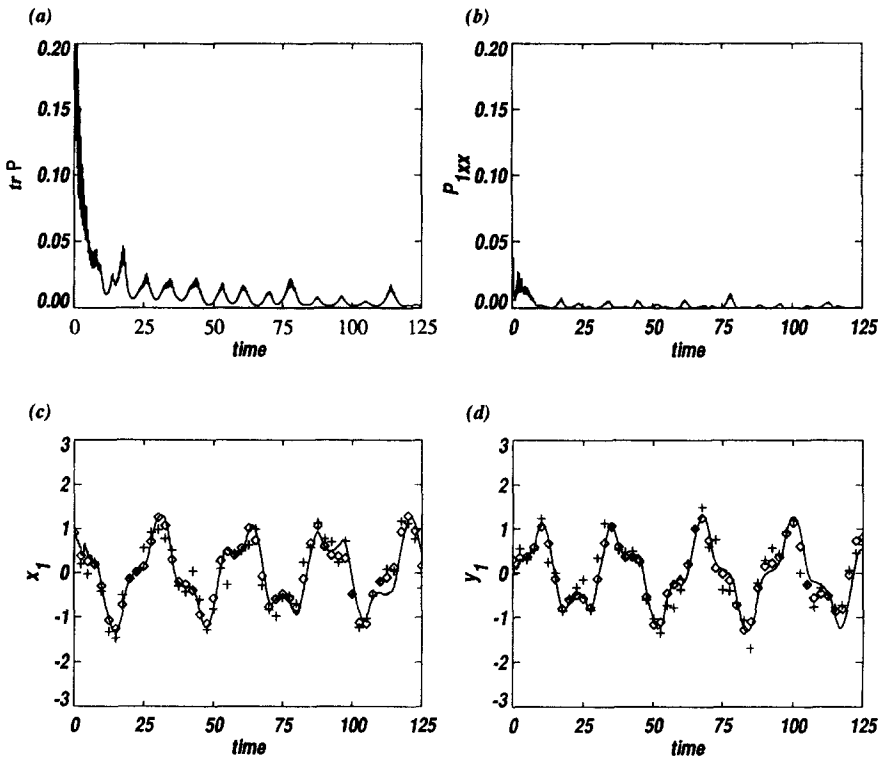

Fig. 9. The performance of the EKF for four point vortices without stochastic forcing, when observing their positions every 0.5 time units. Same panel conventions as in Fig. 2.

When the system is updated frequently using observations of all four vortex positions, the EKF performs well, as shown in Fig. 9 where the system is updated every 0.5 time units. The difference between the true and estimated state may grow rapidly during each forecast interval. The update time interval is chosen therefore to permit tracking the deterministically chaotic vortex trajectories, i.e. it corresponds roughly to the characteristic time of significant trajectory changes (see also Miller et al., 1994).

Because the system is updated quite frequently and the **P**-components decay at every update, the estimated positions evolve mainly due to vortex interaction after the initial adjustment interval. Recall that adding velocity observations did not have a significant impact on the overall EKF performance for two point vortices in the absence of stochastic forcing. However, due to the sensitive dependence on the initial data for the present system of four point vortices, adding an inaccurate velocity observation may result in the actual failure of the EKF, as shown in Fig. 10 where u_1 is added to the four vortex-position observations.

Observing fewer vortex positions may also result in divergence of the estimate from the true state. Since the unobserved vortices are affected significantly less by the updates, the whole system may follow a totally different trajectory due to its sensitivity. In this case adding Eulerian velocity observations can help improve the performance of

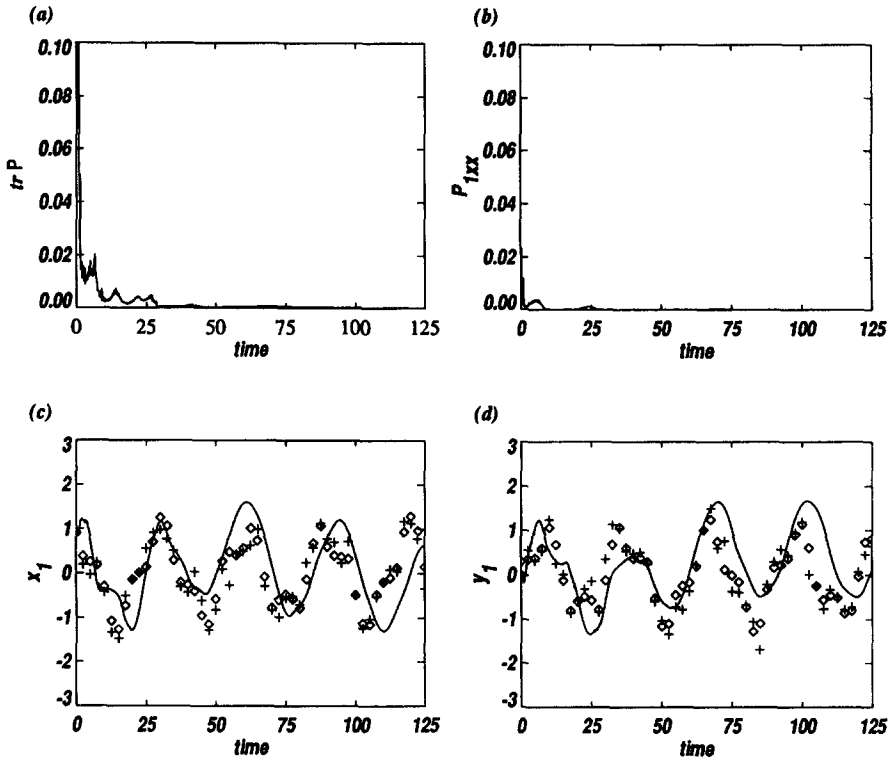

Fig. 10. Same as Fig. 9, but with an additional velocity observation u_1.

the EKF because the update using station velocity has some impact on all the vortices (not shown). The performance of the EKF seems to improve as the number of stations increases, as long as not all vortex positions are observed. Still, adding a few velocity observations does not seem to achieve the same EKF accuracy as when observing all four vortex positions even though the magnitude of the error covariance relative to the corresponding autocovariance is similar for the two types of measurements.

On the whole, absence of random model errors is both unrealistic and detrimental to filter performance. The filter's sensitivity to the number, nature, and accuracy of observations is increased by the chaotic nature of the motion.

3.2.2. With stochastic forcing

In the presence of random model errors, the components of **P** grow much faster and hence each observation has more impact in estimating the vortex positions. When all four vortices are observed, the EKF updates their positions close to the observed values. Even when the interval between updates is longer (2.5 time units, not shown), the update brings all vortex positions close to the observations. Note that the dynamics of z_v^f and z_v^t during each forecast interval may still be rather different.

When three out of four vortex positions are observed, the EKF performs reasonably

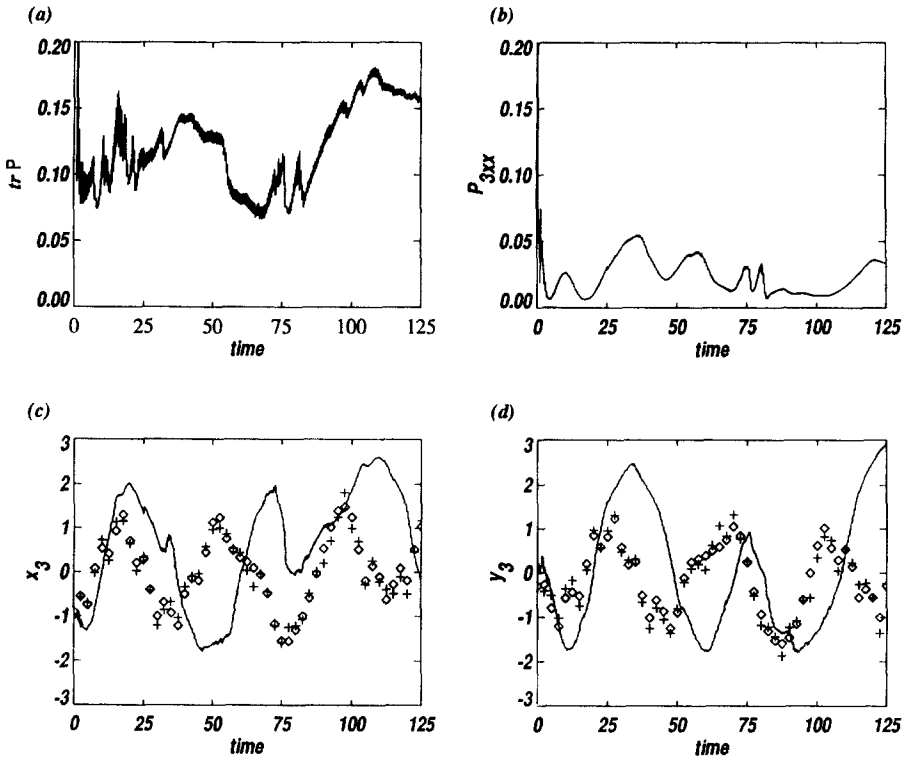

Fig. 11. The performance of the EKF for four point vortices, when observing two vortex positions $\{c_1, c_2\}$ and one velocity u_1 every 0.5 time units, with stochastic forcing: (a) $tr\mathbf{P}$; (b) $P_{3x_3x_3}$; (c) x_3; (d) y_3.

well (not shown). However, observing two vortex positions only seems to result in failure as shown in Fig. 11, where the system is updated every 0.5 time units. The observed vortices recover their observed positions at update time, while the unobserved vortices continue to drift away from their true positions. Adding more velocity observations does not necessarily help EKF performance, due to the nonlinearity of the observation function $\mathbf{H}_s$ in Eq. (9c) (see next section).

In Part II we examine the efficacy of updates using nonlinear, Eulerian observations in greater detail. We skip here many additional experiments with point-vortex systems and proceed instead with a simple analysis that will help us summarize their conclusions.

4. Analysis

4.1. Observation types

In this section, we analyze the update mechanism when using various types of observations common to the system under consideration. This analysis gives geometrical insight into the updating process, based on the Lagrangian representation of the system's

dynamics. It also points out the potential problems in tracking the vortices in the light of the nature of the observations.

Observations in general can be classified first into Lagrangian and Eulerian: the observation function $\mathbf{h}_v$ for vortex position is Lagrangian and the observation function $\mathbf{h}_s$ for velocity at a station is Eulerian. Some observations are functions of only one state variable and others depend on more than one state variables: each $\mathbf{h}_v$ is a function of a single vortex only, while any $\mathbf{h}_s$ depends on the positions of all the vortices. Furthermore, each $\mathbf{h}_v$ is a linear function of one state variable, while any $\mathbf{h}_s$ is a nonlinear function of all state variables. Finally the observations may or may not be represented by analytic functions of state variables when state variables are in complex form: both $\mathbf{h}_v$ and $\mathbf{h}_s$ are analytic functions; not any scalar observation, however, is an analytic function of the state.

Motivated by the fact that both state variables and observations used in this study can be expressed as complex analytic functions, we develop a simple update formalism valid for both Lagrangian and Eulerian data, and for linear as well as nonlinear observation functions. The formalism can also be carried out for nonanalytic observation functions, although the simple geometric interpretation is lost in that case. Use of complex analytic observation functions is consistent with this study because the Laplacian relation between stream function and vorticity is equivalent to a Cauchy–Riemann relation for the velocity components, while incompressibility of the flow gives another such Cauchy–Riemann relation (e.g. Ghil and Balgovind, 1979).

Since the Laplacian is a linear operator, some observation functions can be written as a superposition of functions each of which depends on one vortex only. We define a 'single-state-variable function' (SSVF) as a function which depends on only one of the state variables, such as the observation function for a vortex position. Functions that depend on more than one state variable will be called 'multi-state-variable functions' (MSVFs). There are two classes of MSVF, depending on whether or not they can be written as a superposition of SSVFs. The velocity observation function at a station is an example of MSVF which is a superposition of SSVFs. Although it has not been used in the numerical study of the preceding section, the pressure measured at a station is an MSVF observation which is not a superposition of SSVFs. In this paper we mainly deal with observations represented by analytic SSVFs or MSVFs that are superpositions of analytic SSVFs (simply SSVF and MSVF hereafter, unless otherwise noted).

We analyze first the update mechanism using SSVF observations only in Section 4.2. The geometric representations show the update using observations which are a linear function of state variables to be superior to the update using nonlinear observations: they also highlight the two possible problems noted in Section 3. We analyze next the updates using MSVF data in Section 4.3; this shows how observational data interact during the update.

4.2. Updates using single-state-variable functions (SSVFs)

In this subsection, we examine the update mechanism using an observation function h_k which is a complex analytic SSVF of $z_{v,l}$ of the form

$$h_k = h_k(z_{v,l} - z_{s,k}). \tag{11}$$

This form can describe not only Eulerian data regarding vortex l measured at $z_{s,k}$ but also Lagrangian data by setting $z_{s,k} = 0$.

For simplicity, we assume that block elements of $\mathbf{P}^f$ have the form,

$$\mathbf{P}^f_{mn} = \delta_{mn} p^f_n \mathbf{I}_2 . \tag{12}$$

During actual estimation using the EKF, $\mathbf{P}^f$ takes a more complicated form, but this one is chosen to highlight the underlying update mechanism. It is equivalent to assuming that updates using h_k are restricted to affect $z_{v,l}$ only and do not influence other state variables. Updates using more than one observation of this type are equivalent to repeated updates using one observation at a time. This is a particular instance of sequential processing of observations (Gelb, 1974, Ghil and Malanotte-Rizzoli, 1991). Furthermore, we assume r_k in Eq. (10) to be constant in the present analysis; more generally, r_k can also be a function of the observation magnitude. The analysis can be carried out for such r_k and the main results for the update mechanism remain the same.

Making use of analyticity (Appendix A),

$$\mathbf{P}^a_{mn} = \delta_{mn} p^a_m \mathbf{I}_2 , \tag{13a}$$

$$p^a_m = \begin{cases} \dfrac{r_k}{p^f_l d^2_{kl} + r_k} p^f_l , & \text{if } m = l, \\ p^f_l , & \text{if } m \neq l, \end{cases}$$

$$z^a_{v,l} = z^f_{v,l} + \Delta z_{v,l}, \tag{13b}$$

$$\Delta z_{v,l} = \frac{p^f_l}{p^f_l + r_k / d^2_{kl}} \left(b^o_k - h_k \right) \Big/ \frac{\partial h_k}{\partial z_{v,l}} .$$

Eq. (13a) for $\mathbf{P}^a$ indicates that the update is performed so as to minimize the expected estimation error based on the 'first guess' $h_k(z^f_{v,l} - z_{s,k})$, with error variance given as $p^f_l d^2_{kl}$, and on the actual observation b^o_k, with error variance r_k.

To give a physical and geometric interpretation of $\Delta z_{v,l}$ we first define $z^o_{v,kl}$ implicitly by

$$b^o_k = h_k\left(z^o_{v,kl} - z_{s,k} \right). \tag{14}$$

By this definition, $z^o_{v,kl} = z_{s,k} - h_k^{-1}(b^o_k)$ is the 'observed' position of vortex l obtained from the observation b^o_k assuming that the observation contains no error. In all the cases considered here the function h_k can be inverted explicitly, using algebraic manipulations and background knowledge about the vortices' positions; the following applies whenever h_k^{-1} does exist. More generally, if there exists more than one root for $z^o_{v,kl}$, we choose the one which is closest to $z^f_{v,l}$ Substituting Eq. (14) into Eq. (13b), the EKF update places $z^a_{v,l}$ between and $z^f_{v,l}$ and $z^o_{v,kl}$, with $z_{s,k}$ as pivot point:

$$\Delta z_{v,l} = \frac{p^f_l d^2_{kl}}{p^f_l d^2_{kl} + r_k} \left\{ h_k\left(z^o_{v,kl} - z_{s,k} \right) - h_k\left(z^f_{v,l} - z_{s,k} \right) \right\} \Big/ \frac{\partial h_k}{\partial z_{v,l}} . \tag{15}$$

This is consistent with Eq. (13a) and can be thought of as Newton's method for the solution of Eq. (14).

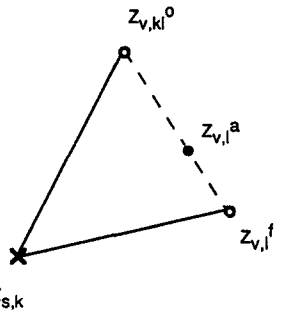

Fig. 12. Geometric representation of the update mechanism when using a vortex-position observation ($\gamma = 1$ in Eq. (16)).

Motivated by the form of the observation functions used in the numerical study, let us take

$$h_k(z_{v,kl}^o - z_{s,k}) = a_l(z_{v,kl}^o - z_{s,k})^\gamma. \tag{16}$$

where a_l is a complex constant and γ is an integer. For example, $\gamma = 1$ corresponds to the observation function for the position of vortex l with respect to station k and $\gamma = -1$ corresponds to the velocity at station k induced by vortex l.

For $\gamma = 1$, Eq. (13b) becomes

$$\Delta z_{v,l} = \frac{p_l^f}{p_l^f + r_k/d_{kl}^2}(z_{v,kl}^o - z_{v,l}^f), \tag{17}$$

with $d_{kl}^2 = 1$ from Eq. (A2). This is equivalent to updating $z_{v,l}^f$ with $z_{v,kl}^o$, based on error variances p_l^f and r_k/d_{kl}^2, respectively; $z_{v,l}^f$ is updated to $z_{v,l}^a$ as shown in Fig. 12.

For $\gamma = -1$,

$$\Delta z_{v,l} = \frac{p_l^f}{p_l^f + r_k/d_{kl}^2}(z_{v,kl}^o - z_{v,l}^f)\frac{z_{v,l}^f - z_{s,k}}{z_{v,kl}^o - z_{s,k}}. \tag{18}$$

Fig. 13(a)–(c) show the geometric interpretation $\Delta z_{v,l}$ is obtained through magnifying $(z_{v,kl}^o - z_{v,l}^f)$ by the factor $A_{kl} \equiv |(z_{v,l}^f - z_{s,k})/(z_{v,kl}^o - z_{s,k})|$, applying the statistical weight $p_l^f/(p_l^f + r_k/d_{kl}^2)$, and rotating by the angle ϕ defined by $(z_{v,kl}^o - z_{s,k} - z_{v,l}^f)$ (Fig. 13(a)). The term $(z_{v,l}^f - z_{s,k})/(z_{v,kl}^o - z_{s,k})$ represents the nonlinearity of the observation and provides the magnification and rotation. When the first guess $z_{v,l}^f$ is moderately far away from the location $z_{s,k}$ of the station, while both dynamical and observational errors are of comparable size and not too large, then $z_{v,l}^f$ and $z_{v,kl}^o$ are expected to be closer to each other than to $z_{s,k}$. Hence the angle ϕ is expected to be small and $A_{kl} \sim \mathcal{O}(1)$. As a result, the analyzed position $z_{v,l}^a$ is expected to be in the neighborhood of $z_{v,l}^f$ and $z_{v,kl}^o$ (Fig. 13(b)).

There are two cases in which the update may fail to improve the estimated position of a vortex for $\gamma = -1$. First, when $z_{v,l}^f$ and $z_{v,kl}^o$ are both close to $z_{s,k}$—i.e. within distance $\sqrt{p_l^f}$ and $\sqrt{r_k/d_{kl}^2}$, respectively—the EKF update may deteriorate the estimate due to the following reason. Since the function h_k is singular at $z_{s,k}$, cf. Eq. (16), the

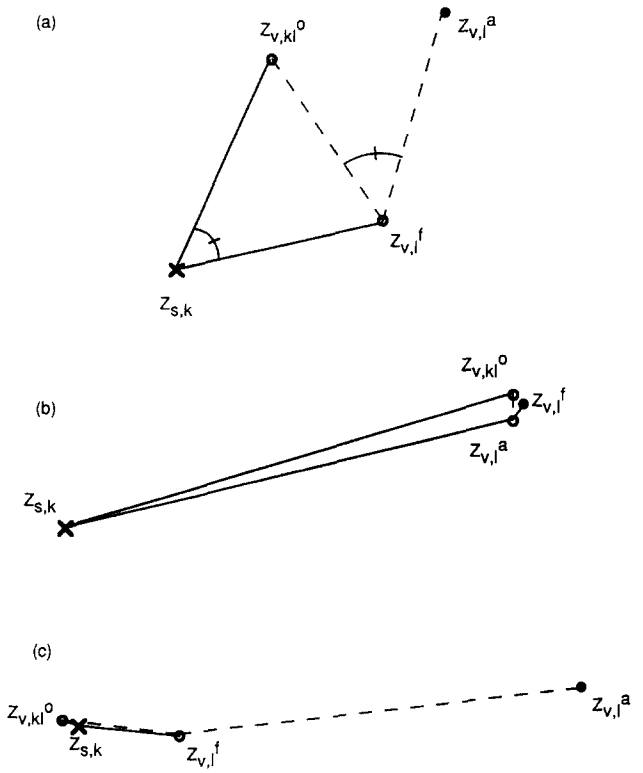

Fig. 13. Geometric representation of the update mechanism when using station velocity observations ($\gamma = -1$). See text for explanation of panels (a), (b), and (c).

'observed' vortex position $z_{v,kl}^o$ is expected to be located close to the true vortex position. Hence the update is optimal when the nonlinear effect is weak, i.e. when

$$\frac{z_{v,l}^f - z_{s,k}}{z_{v,kl}^o - z_{s,k}} \sim 1.$$

The update fails when the nonlinear contribution is significant. For $\gamma = -1$, this occurs when the 'observed' vortex is too close to the station and ϕ is larger than $\pi/2$ (Fig. 13(c)). Once the EKF loses track of a vortex through this mechanism, the recapture of the vortex after it moves away from the station is unlikely because of the nonlinearity. Numerical experiments with the full model (not shown in Section 3, for the sake of brevity) confirm this analysis.

The second case occurs when the true vortex $z_{v,l}^t$ is far away from the station (see Fig. 2 of Part II), or the station lies near a stagnation point (recall Fig. 5), and hence the magnitude of $h_k(z_{v,l}^t - z_{s,k})$ is very small. In this case, even a small error in the observation b_k^o can easily result in $z_{v,kl}^o$ lying on the opposite side of $z_{s,k}$ and away from $z_{v,l}^t$ (cf. Eqs. (14) and (16)), resulting in a poor estimate of $\Delta z_{v,l}$.

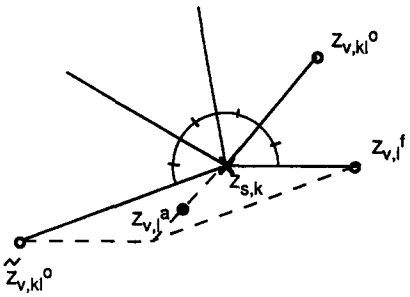

Fig. 14. Geometric representation of the update mechanism for $\gamma \geq 2$.

In general, $\Delta z_{v,l}$ has the following form

$$\Delta z_{v,l} = \frac{p^{f}_{l}}{p^{f}_{l} + r_k/d^{2}_{kl}} \frac{1}{\gamma} \left\{ \left(z^{o}_{v,kl} - z_{s,k} \right) \left(\frac{z^{o}_{v,kl} - z_{s,k}}{z^{f}_{v,l} - z_{s,k}} \right)^{\gamma - 1} - \left(z^{f}_{v,l} - z_{s,k} \right) \right\}. \quad (19)$$

Fig. 14 demonstrates the update mechanism for $\gamma > 1$ with $\gamma = 4$. We define the 'modified observed' position $\tilde{z}^{o}_{v,kl}$ of vortex l as

$$\tilde{z}^{o}_{v,kl} = z_{s,k} + \left(z^{o}_{v,kl} - z_{s,k} \right) \left(\frac{z^{o}_{v,kl} - z_{s,k}}{z^{f}_{v,l} - z_{s,k}} \right)^{\gamma - 1}. \quad (20)$$

With this definition, Eq. (19) becomes equivalent to the update of $z^{f}_{v,l}$ by $\tilde{z}^{o}_{v,kl}$ using variances p^{f}_{l} and r_k/d^{2}_{kl}, respectively. Similarly, for $\gamma < -1$, the update is illustrated geometrically in Fig. 15. For both $\gamma > 1$ and $\gamma < -1$, the quality of the update depends on how accurately $\tilde{z}^{o}_{v,kl}$ represents the true vortex position.

Among the two failure mechanisms illustrated for $\gamma = -1$, the former one, i.e. when vortices are too close to the station, applies to both $\gamma \geq 2$ and $\gamma \leq -2$. If $z^{f}_{v,l}$ is too close to the station $z_{s,k}$, then the nonlinearity leads to failure of the update, since $\tilde{z}^{o}_{v,kl}$ may no longer approximate well the position of vortex l. Any nonlinear observations,

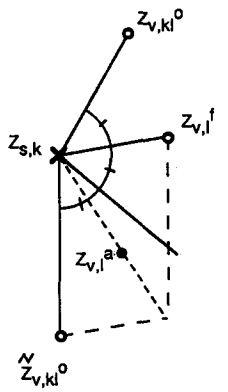

Fig. 15. Geometric representation of the update mechanism for $\gamma \leq -2$.

$\gamma \neq 1$, can thus be detrimental to the tracking when the vortices get too close to the stations at observation time. On the other hand, the latter mechanism, i.e. near-zero observation, can arise only for $\gamma \leq -1$.

4.3. Updates using multi-state-variable functions (MSVFs)

The analysis of MSVF updates is more complicated in general than that of SSVFs. In order to illustrate their essence, we use two complex state variables, $z_{v,1}$ and $z_{v,2}$, and two MSVFs. This is the simplest case in which the observations interact and one bad observation may affect negatively the whole update. For this simple system, $\mathbf{P}^f$ is assumed to have the same form as in the previous section and the h_ks ($k = 1, 2$) are assumed to be MSVFs of both $z_{v,1}$ and $z_{v,2}$,

$$h_k = \sum_{l=1}^{2} h_{kl}(z_{v,l} - z_{s,k}), \quad k = 1,2. \tag{21}$$

The corresponding matrix $\mathbf{H}$ is

$$\mathbf{H} = \begin{pmatrix} Gh'_{11} & Gh'_{12} \\ Gh'_{21} & Gh'_{22} \end{pmatrix}, \tag{22a}$$

where

$$Gh'_{kl} = \begin{pmatrix} \mathscr{R} & -\mathscr{I} \\ -\mathscr{I} & -\mathscr{R} \end{pmatrix} h'_{kl}, \tag{22b}$$

$$h'_{kl} = \frac{\partial h_k}{\partial z_{v,l}}.$$

Making use of the analyticity of the functions involved, the gain matrix $\mathbf{K}$ and estimation-error covariance $\mathbf{P}^a$ are obtained as in Appendix B. The analysis vector z_v^a is given by

$$z_v^a = z_v^f + \Delta z_v \tag{23a}$$

$$\begin{pmatrix} \Delta z_{v,1} \\ \Delta z_{v,2} \end{pmatrix} = \frac{1}{\alpha} \begin{pmatrix} p_1^f d_{11}^2 (p_2^f d_{22}^2 + r_2) \dfrac{\Delta b_1}{h'_{11}} - p_1^f d_{21}^2 (p_2^f d_{12}^2 + r_2) \dfrac{\Delta b_1}{h'_{12}} \dfrac{h'_{22}}{h'_{21}} \\ \quad + p_1^f d_{21}^2 (p_1^f d_{21}^2 + r_1) \dfrac{\Delta b_2}{h'_{21}} - p_1^f d_{11}^2 (p_2^f d_{22}^2 + r_2) \dfrac{\Delta b_2}{h'_{22}} \dfrac{h'_{12}}{h'_{11}} \\ p_2^f d_{12}^2 (p_1^f d_{21}^2 + r_1) \dfrac{\Delta b_1}{h'_{12}} - p_2^f d_{22}^2 (p_2^f d_{12}^2 + r_2) \dfrac{\Delta b_1}{h'_{22}} \dfrac{h'_{21}}{h'_{22}} \\ \quad + p_1^f d_{11}^2 (p_2^f d_{22}^2 + r_2) \dfrac{\Delta b_2}{h'_{22}} - p_2^f d_{12}^2 (p_1^f d_{11}^2 + r_1) \dfrac{\Delta b_2}{h'_{21}} \dfrac{h'_{11}}{h'_{12}} \end{pmatrix} \tag{23b}$$

where

$$\Delta b_k = b_k^o - h_k(z_v^f) \tag{23c}$$

and the scaling factor α in Eq. (23b) is given in Appendix B. The first and third terms in $\Delta z_{v,l}$ are the direct corrections to $z_{v,l}$ due to b_1^o and b_2^o, respectively. The second and fourth terms are indirect corrections due to the correction in the position of the other vortices by b_1^o and b_2^o, respectively, i.e. although $z_{v,1}$ and $z_{v,2}$ are independent variables, their updates interact because h_k depends on both. For example, the second term of $\Delta z_{v,1}$ is

$$\frac{b_1^o - h_1}{h'_{12}} \frac{h'_{22}}{h'_{21}} = \frac{b_1^o - h_1}{h'_{12}} \left. \frac{\partial z_{v,2}}{\partial z_{v,1}} \right|_{h_2}.$$

By analogy with the definition of $z^o_{v,kl}$ in the previous subsection, we define a new 'observed' position $z^o_{kj}|_l$ of vortex j as follows

$$z^o_{kj}|_l = \begin{cases} z^f_{v,j}, & \text{if} \quad j \neq l, \\ z_{s,k} - h_{kl}^{-1}\left\{ b_k^o - \sum_{j=1, j\neq 1}^{2} h_{kj}\left(z_{s,k} - z^f_{v,j} \right) \right\}, & \text{if} \quad j = 1; \end{cases} \tag{24}$$

$z^o_{kl}|_l$ is the position of vortex l obtained from $b_k^o = \sum_{j=1}^{2} h_{kj}(z_{s,k} - z^o_{kj}|_l)$ by assuming that the other vortex is at its forecast position and that the observation contains no error. This definition allows us to eliminate the influence of the other vortex from the observation and examine the update of vortex l only, so that Δb_k in Eq. (23c) becomes

$$\Delta b_k = h_k\left(z_{s,k} - z^o_{kl}|_l \right) - h_k\left(z_{s,k} - z^f_{v,l} \right).$$

For h_k having the same form as in Eq. (16), $\Delta \mathbf{z}_v$ gives a geometric interpretation similar to that in the previous subsection. The interpretation of the first and third terms in $\Delta z_{v,l}$ is therewith the same as in the previous subsection. The second and fourth terms are slightly more subtle. For example, the second term in $\Delta z_{v,1}$ has an extra rotation and magnification due to $h'_{22}/h'_{21} = \{(z_{s,k} - z^f_{v,2})/(z_{s,k} - z^f_{v,1})\}^{\gamma-1}$. Note that if the update of one vortex is not sufficiently accurate, then the update of the other vortex is not likely to be very accurate either, due to interaction in the update process.

The two potential problems discussed for SSVFs with $\gamma = -1$ also apply to the update using MSVFs, i.e. close approach of a vortex to a station when using velocity observations for $\gamma \neq 1$ and near-zero-velocity observations for $\gamma \leq -1$. These problems in EKF tracking when using nonlinear Eulerian observations can be overcome by eliminating the l^{-4} singularity in the Rankine-vortex method, on the one hand, and applying a cut-off threshold to near-zero observations for $\gamma \leq -1$, on the other (cf. Part II).

5. Summary and discussion

The extended Kalman filter (EKF) was used on point-vortex systems to investigate the performance of data assimilation for nonlinear flow dynamics representing coherent structures in a Lagrangian framework. Various types of observations were used, including Eulerian, Lagrangian, linear and nonlinear data. Numerical as well as analytical results were obtained.

In the numerical study, EKF performance was tested for both regular and chaotic systems, in the absence and presence of stochastic forcing. Successful tracking of the point vortices using the EKF depends on the balanced performance of the dynamical (forecast) and statistical (optimization) steps in the filtering process. When initial data are properly given and (Lagrangian) vortex observations are made frequently and accurately, tracking is excellent (Fig. 2). When observations are less plentiful or accurate (Fig. 3), absence of stochastic forcing tends to yield insufficient gain for the updates, whether the system is chaotic (cf. also Miller et al., 1994) or regular. This problem does not arise under the more realistic assumption that random model errors, representing subgrid-scale processes are present (Fig. 7).

Numerical results show that observing all vortex positions in the system provides the best performance in general. When this is the case, other types of observations may improve marginally the performance of the EKF for a system whose underlying dynamics is regular and may actually deteriorate it for chaotic system (Fig. 10). The contribution of velocity observations depends on a number of factors. Their most useful aspect is that one velocity observation updates all the vortex positions in the flow, while a vortex-position observation only updates the corresponding vortex. Their most important drawback is that the impact of such and observation on the update behaves like l^{-4}, where l is the distance between the station in question and the updated point vortex; hence the effect is strongly singular for $l \ll 1$ and very weak for $l \gg 1$. For an insufficient number of vortex-position observations, there are situations where the contribution of velocity observations may be deleterious, due to their nonlinear character and to the interaction between observations.

A simple analysis of the update mechanism exploited sequential processing of observations (Ghil and Malanotte-Rizzoli, 1991, Section 5.3.1) and the analytic nature of the observation functions in this idealized data assimilation problem. It illustrates the update process geometrically in terms of rotations and stretchings of vectors in polygons spanned by the vortex and station positions. The analysis indicates that linear, Lagrangian observations of vortex positions are preferable, in general, to nonlinear, Eulerian velocity observations, and emphasizes the role of singularities of the observing function in loss of tracking when point vortices approach too closely a velocity-observing station. As shown in Part II, however, nonlinear, Eulerian observations can be as informative and useful as linear, Lagrangian ones if the overall tracking system is judiciously designed.

This singularity in the Eulerian observing function, and the ensuing loss of tracking, appear to be due to the artificial singularity of the velocity profile in a point vortex. To remove the latter, and hopefully the former singularity, we consider in Part II systems of Rankine vortices, with a finite-radius core in solid-body rotation and a potential flow exterior.

Acknowledgements

This paper is dedicated to the contribution of Richard L. Pfeffer to the applications of geophysical fluid dynamics (GFD) to large-scale atmospheric and oceanic motions:

vortices are fundamental to GFD and we hope they will prove useful in data assimilation. It is a pleasure to thank A. Mariano, A. Robinson, and N. Zabusky for suggesting, directly or indirectly, and at different times, the problem to the authors. The presentation was greatly improved by detailed comments from R. Daley and three anonymous reviewers. This work was supported by ONR Grant N0014-93-J-0673 and NASA Grant NAG-5713 (KI and MG) and by the Condorcet Visiting Chair of the Ecole Normale Supérieure, Paris (MG). This is IGPP contribution no. 4603.

Appendix A. Derivation of SSVF results

Because h_k is an analytic function, the $2 \times 2N$ elements of $\mathbf{H}$ in Eq. (14) are written in complex form as

$$\mathbf{H}_{ln} = \begin{cases} 0, & \text{if } n \neq l, \\ G\left(\dfrac{\partial h_k}{\partial z_{v,l}} \right), & \text{if } n = l, \end{cases} \quad \mathbf{H}^T_{ln} = \begin{cases} 0, & \text{if } n \neq l \\ G\left(\dfrac{\partial h_k}{\partial z_{v,l}} \right)^* = G\left(d^2_{kl} / \dfrac{\partial h_k}{\partial z_{v,l}} \right), & \text{if } n = l; \end{cases} \tag{A1}$$

here

$$d^2_{kl} = \left| \frac{\partial h_k}{\partial z_{v,l}} \right|^2 \tag{A2}$$

and G is an operator defined in Eqs. (22a) and (22b). The matrix operation with $\mathbf{H}$ involving G in Eqs. (5a), (5b) and (5c) is equivalent to complex variable manipulation while dropping G. The block element of the $2N \times 2$ gain matrix $\mathbf{K}$ is then given by

$$\mathbf{K}_{ln} = \begin{cases} 0, & \text{if } n \neq l, \\ G\left(\dfrac{p^f_l}{p^f_l + r_k / d^2_{kl}} \Big/ \dfrac{\partial h_k}{\partial z_{v,l}} \right), & \text{if } n = l. \end{cases} \tag{A3}$$

Substitution of Eqs. (A1) and (A3) into Eq. (5a) results in Eqs. (13a) and (13b). For a station-velocity observation,

$$d^2_{kl} = \left| \frac{\Gamma_l}{2\pi} \frac{1}{(z_{v,l} - z_{s,k})^2} \right|^2 \sim |z_{v,l} - z_{s,k}|^{-4}, \tag{A4}$$

hence the impact of the update behaves like $|z_{v,l} - z_{s,k}|^{-4}$.

Appendix B. Derivation of MSVF results

After some algebra using both G matrix operations and complex variable manipulation, the 4×4 gain matrix $\mathbf{K}$ becomes

$$\mathbf{K} = \begin{pmatrix} Gk_{11} & Gk_{12} \\ Gk_{21} & Gk_{22} \end{pmatrix}, \tag{B1}$$

where

$$
\begin{aligned}
k_{11} &= \frac{1}{\alpha}\left\{ p_1^{\mathrm{f}} d_{11}^2 \left(p_2^{\mathrm{f}} d_{22}^2 + r_2 \right) \frac{1}{h'_{11}} - p_1^{\mathrm{f}} d_{21}^2 \, p_2^{\mathrm{f}} d_{12}^2 \frac{h'_{22}}{h'_{21} h'_{12}} \right\}, \\
k_{12} &= \frac{1}{\alpha}\left\{ p_2^{\mathrm{f}} d_{12}^2 \left(p_1^{\mathrm{f}} d_{21}^2 + r_1 \right) \frac{1}{h'_{12}} - p_2^{\mathrm{f}} d_{22}^2 \, p_1^{\mathrm{f}} d_{11}^2 \frac{h'_{21}}{h'_{12} h'_{22}} \right\}, \\
k_{21} &= \frac{1}{\alpha}\left\{ p_1^{\mathrm{f}} d_{21}^2 \left(p_2^{\mathrm{f}} d_{12}^2 + r_2 \right) \frac{1}{h'_{21}} - p_1^{\mathrm{f}} d_{11}^2 \, p_2^{\mathrm{f}} d_{22}^2 \frac{h'_{12}}{h'_{11} h'_{22}} \right\}, \\
k_{22} &= \frac{1}{\alpha}\left\{ p_2^{\mathrm{f}} d_{22}^2 \left(p_1^{\mathrm{f}} d_{11}^2 + r_1 \right) \frac{1}{h'_{22}} - p_2^{\mathrm{f}} d_{12}^2 \, p_1^{\mathrm{f}} d_{21}^2 \frac{h'_{11}}{h'_{12} h'_{21}} \right\},
\end{aligned}
\tag{B2}
$$

p_k^{f} is defined in Eq. (11), r_k^{f} in Eqs. (13a) and (13b), d_{kl} in Eq. (A2), h'_{kl} in Eqs. (22a) and (22b), and

$$
\alpha = \left(p_1^{\mathrm{f}} d_{11}^2 + p_2^{\mathrm{f}} d_{12}^2 + r_1 \right)\left(p_1^{\mathrm{f}} d_{21}^2 + p_2^{\mathrm{f}} d_{22}^2 + r_2 \right) - \left| p_1^{\mathrm{f}} d_{11}^2 \frac{h'_{21}}{h'_{11}} + p_2^{\mathrm{f}} d_{22}^2 \frac{h'_{22}}{h'_{12}} \right|^2 \tag{B3}
$$

Using $\mathbf{K}$, we compute the analysis error covariance $\mathbf{P}^{\mathrm{a}}$

$$
\mathbf{P}^{\mathrm{a}} = [\mathbf{I}_4 - \mathbf{KH}]\mathbf{P}^{\mathrm{f}} \tag{B4}
$$

where

$$
\mathbf{KH} = \frac{1}{\alpha}\begin{pmatrix} G(kh)_{11} \\ G(kh)_{12} \end{pmatrix} \tag{B5}
$$

$$
\begin{aligned}
\begin{pmatrix} (kh)_{11} \\ (kh)_{12} \end{pmatrix} = \Bigg(& p_1^{\mathrm{f}} d_{11}^2 \left(p_2^{\mathrm{f}} d_{22}^2 + r_2 \right) - p_1^{\mathrm{f}} d_{21}^2 \, p_2^{\mathrm{f}} d_{12}^2 \frac{h'_{22} h'_{11}}{h'_{21} h'_{12}} + p_1^{\mathrm{f}} d_{21}^2 \left(p_2^{\mathrm{f}} d_{12}^2 + r_2 \right) \\
& - p_1^{\mathrm{f}} d_{11}^2 \, p_2^{\mathrm{f}} d_{22}^2 \frac{h'_{12} h'_{21}}{h'_{11} h'_{22}} p_2^{\mathrm{f}} d_{12}^2 \left(p_1^{\mathrm{f}} d_{21}^2 + r_1 \right) - p_2^{\mathrm{f}} d_{22}^2 \, p_1^{\mathrm{f}} d_{11}^2 \frac{h'_{21} h'_{12}}{h'_{12} h'_{22}} \\
& + p_2^{\mathrm{f}} d_{22}^2 \left(p_1^{\mathrm{f}} d_{11}^2 + r_1 \right) - p_2^{\mathrm{f}} d_{12}^2 \, p_1^{\mathrm{f}} d_{21}^2 \frac{h'_{11} h'_{11}}{h'_{12} h'_{21}} \Bigg).
\end{aligned}
\tag{B6}
$$

The form of $\mathbf{KH}$ shows the interaction between observations and state variables.

References

Anderson, J.L., 1995. Selection of initial conditions for ensemble forecasts in a simple perfect framework. J. Atmos. Sci. 53, 22–36.

Aref, H., 1984. Integrable, chaotic, and turbulent vortex motion in two-dimensional flow. Ann. Rev. Fluid Mech. 15, 345–389.

Bengtsson, L., Ghil, M., Källén, E. (Eds.), 1981. Dynamic Meteorology: Data Assimilation Methods, Appl. Math. Sci. Ser. Vol. 36. Springer-Verlag, 330 pp.

Buizza, R., Tribbia, J., Molteni, F., Palmer, T., 1993. Computation of optimal unstable structures for a numerical weather prediction model. Tellus 45A, 388–406.

Cohn, S., 1993. Dynamics of short-term univariate forecast error covariance. Won. Weather Rev. 121, 3123–3149.

Daley, R., 1991. Atmospheric Data Analysis. Cambridge University Press, 420 pp.

Gelb, A. (Ed.), 1974. Applied Optimal Estimation. The MIT Press, 374 pp.

Gandin, L.S., 1965. Objective Analysis of Meteorological Fields (Israel Program for Scientific Translations, Jerusalem, Trans.). Gidrometeorol. Izd., 242 pp. (original work published 1963).

Ghil, M., 1989. Meteorological data assimilation for oceanographers. Part I: Description and theoretical framework. Dyn. Atmos. Oceans 13 (3-4), 171–218.

Ghil, M., Balgovind, R., 1979. A fast Cauchy–Riemann solver. Math. Comput. 33, 585–635.

Ghil, M., Ide, K., 1994. Extended Kalman filtering for vortex systems: an example of observing system design. In: Brasseur, P., Nihoul, J.C.J. (Eds.), Data Assimilation for Modelling Ocean in a Global Change Perspective. Springer-Verlag, New York, pp. 167–193.

Ghil, M., Malanotte-Rizzoli, P., 1991. Data assimilation in meteorology and oceanography. Adv. Geophys. 33, 141–226.

Ghil, M., Cohn, S.E., Taventzis, J., Bube, K., Isaccson, E., 1981. Application of estimation theory to numerical weather prediction. In: Bengtsson, L., Ghil, M., Källén, E. (Eds.), Dynamic Meteorology: Data Assimilation Methods, Appl. Math. Sci. Ser. Vol. 36. Springer-Verlag, pp. 139–224.

Greenside, H.S., Helfand, H., 1981. Numerical integration of stochastic differential equations – II. Bell Syst. Tech. J. 60, 1927–1940.

Hao, Z., Ghil, M., 1995. Sequential parameter estimation for a coupled ocean–atmosphere model. In: Proceedings of the Second WMO International Symposium on Assimilation of Observations in Meteorology and Oceanography, Tokyo, vol. 1. pp. 181–186.

Ide, K., Ghil, M., 1997a. Extended Kalman filtering for vortex systems. Part II: Rankine vortices and Eulerian data. Dyn. Atmos. Oceans 27, 333–350.

Ide, K., Ghil, M., 1997b. Evolution of prediction errors in nonlinear systems, deterministic and stochastic. (In preparation.)

Jazwinski, A.H., 1970. Stochastic Processes and Filtering Theory. Academic Press, 376 pp.

Kalman, R.E., 1960. A new approach to linear filtering and prediction problems. Trans. ASME, Ser. D, J. Basic Eng. 82D, 35–45.

Kalman, R.E., Bucy, R.S., 1961. New results in linear filtering and prediction problems. Trans. ASME, Ser. D, J. Basic Eng. 83D, 95–108.

Legras, B., Vautard, R., 1996. A guide to Liapunov vectors. In: Palmer, T. (Ed.), Proc. 1995 ECMWF Seminar on Predictability. ECMWF, Reading, UK, pp. 143–156.

Lorenc, A., 1981. A global three-dimensional multivariate statistical interpolation scheme. Mon. Weather Rev. 109, 701–721.

Mariano, A.J., 1990. Contour analysis: a new approach for melding geophysical fields. J. Atmos. Ocean. Tech. 7, 285–295.

McWilliams, J.C., 1980. An application of equivalent modons to atmospheric blocking. Dyn. Atmos. Oceans 5, 43–66.

McWilliams, J.C., 1991. Geostrophic vortices. In: Osborne, A.R. (Ed.), Nonlinear Topics in Ocean Physics: Proceedings of the International School of Physics "Enrico Fermi" Course 109. Elsevier Science Publishers B.V., Amsterdam, pp. 5–50.

Miller, R., Ghil, M., Gauthiez, F., 1994. Advanced data assimilation in strongly nonlinear dynamical systems. J. Atmos. Sci. 51, 1037–1056.

Panel on Model-Assimilated Data Sets for Atmospheric and Oceanic Research, 1991. Four-Dimensional Model Assimilation of Data: A Strategy for the Earth System Sciences. National Academy Press, 78 pp.

Provost, C., Salmon, R., 1986. A variational method for inverting hydrographic data. J. Mar. Res. 44, 1–34.

Robinson, A.R. (Ed.), 1983. Eddies in Marine Science. Springer-Verlag, 609 pp.

Sasaki, Y., 1970. Some basic formalisms in numerical variational analysis. Mon. Weather Rev 98, 875–883.

Smedstad, O.M., O'Brien, J., 1991. Variational data assimilation and parameter estimation in an equatorial Pacific Ocean model. Prog. Oceanogr. 26, 179–241.

Talagrand, O., Courtier, P., 1987. Variational assimilation of meteorological observations with the adjoint vorticity equation. I. Theory. Q.J.R. Meteorol. Sci. 113, 1311–1328.

Toth, K., Kalnay, E., 1993. Ensemble forecasting at NMC: the generation of perturbations. Bull. Am. Met. Soc. 74, 2317–2330.